Lecture 22. Conceptual models for the thermohaline circulation

5/2/2006 9:32 AM

1. Conceptions of thermohaline circulation

Dense deep water, formed at high latitudes, has long been thought as the driving force for the thermohaline circulation in the oceans. This seems a logical extension from what happens in the atmosphere, where solar insolation heats up the low and middle part of the atmosphere, and convection takes place, while the outer space works as the cooling source for this heat engine. Although the atmospheric thermal engine efficiency is very low, on the order of 0.8%, it is a heat engine indeed. The question relevant to oceanography is whether surface cooling can work as a driving force for the thermohaline circulation?

A. **Classical view of thermohaline circulation**.

From the early stage of theoretic development surface thermal forcing has been identified as the driving force for the thermohaline circulation, and the classical picture of thermohaline circulation can be illustrated by the following sketch.

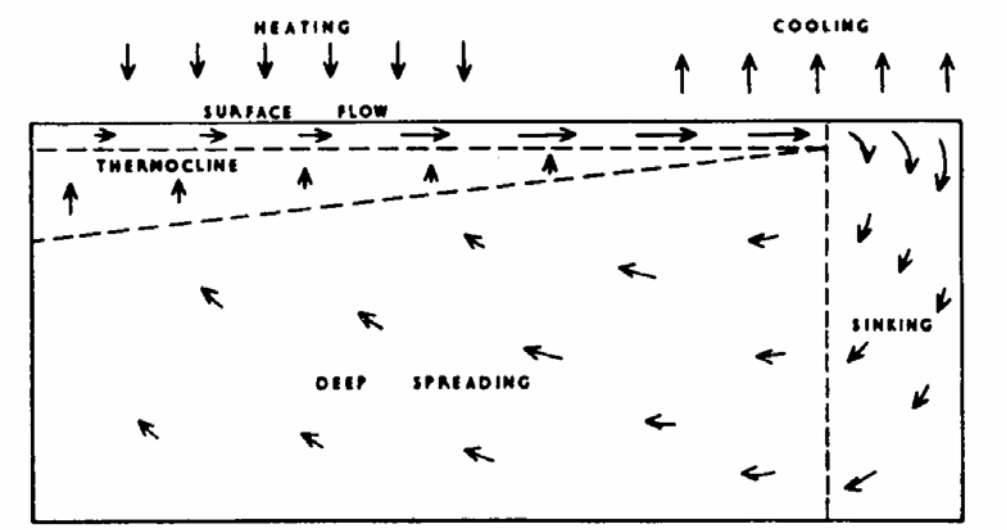

Fig. 1. A classical sketch of thermohaline circulation driven by surface cooling/heating (Wytki, 1961)

Wytki (1971) wrote: "The circulation must take place in a meridional plane between the region of heating in low latitudes and the region of cooling in high latitudes." and he postulated a circulation system consisting of four principal processes:

a. the heating of the surface layer and the poleward flow at the surface,
b. the sinking of heaviest water in highest latitudes,
c. the spreading towards the equator in the deep layer, and
d. the ascending of the deep water through the thermohaline into the surface layer

Note that water mass transformation in his framework takes place in the surface layer only. Accordingly, the circulation described by Wytki requires a surface layer as the essential ingredient of the water cycle where water mass properties are changed by air-sea buoyancy flux, and his discussion was primarily focused on the air-sea heat flux in water mass transformation in the surface layer, and there is no internal mixing required. In his framework, the wind-driven circulation was completely separated from the thermohaline circulation, and he did not mention any potential role of wind stress in

setting up the thermohaline circulation. Thus, in some sense he was talking about the so-called pure thermohaline circulation.

Late on this framework was modified as following: mixing in the surface layer is replaced by diapycnal mixing at the middle depth of the ocean interior. Accordingly, the main balance in the oceanic interior is between the vertical upwelling and the downward heat diffusion, as discussed by Munk (1966). In the modified framework, there is no need for the wind stress because the poleward flow of surface layer is presumably driven by pressure gradient generated by the thermohaline circulation itself, instead of wind stress. Therefore, the circulation would be really a pure thermohaline circulation. Similar to the previous framework, the circulation system consists of four components:

a. Dense water formed at high latitude sinks to the great depth.
b. Dense deep water spreads to the whole basin.
c. Deep water upwells through the base of the main thermocline.
d. Surface water turns poleward and completes the cycle.

B. Three schools of the thermohaline circulation

In order to explain the thermohaline circulation in the oceans, two theories or schools have been proposed. The first one, which has been the one which dominated our thinking about thermohaline circulation, postulated that thermohaline circulation is driven by deep water formation at high latitudes, as shown in Fig. 2a. This will be called school of push.

The second theory postulates that mechanical energy is needed to overcome the friction and thus thermohaline circulation is driven by external sources of mechanical energy, such as tidal dissipation and wind stress. This will be called school of pulling. This is further separated into two sub-schools, as explained in the following discussion.

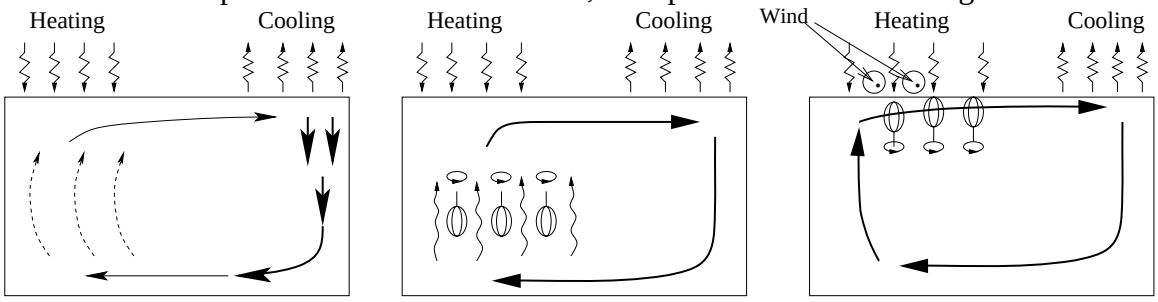

a) Pushing by Deepwater Formation b) Pulling by Deep Mixing c) Pulling by Wind Stress

Fig. 2. Three schools of theory for the thermohaline circulation.

1) School of push: Deepwater formation pushes the deep current and thus maintains the thermohaline circulation.

This is the old school, in which thermohaline circulation is driven by surface thermohaline forcing, in particular the surface cooling/heating. Surface cooling produces dense water that sinks to the great depth. The high latitude ocean is filled up with cold and dense water from surface to bottom. In comparison with the warm and light water in the upper ocean at low latitudes, this creates a pressure force in the abyssal ocean which drives cold bottom water to move towards low latitudes and thus pushing the meridional circulation. Due to the Coriolis force, however, flow does not simply move down

pressure direction; nevertheless, this argument provides a connection between meridional overturning circulation and pressure difference induced by surface thermohaline forcing and deepwater formation.

As will be discussed shortly, Stommel's (1961) classical 2-box model belongs to this category because he assumed that circulation rate is proportional to north-south pressure difference. Most importantly, he assumed that the constant relating the pressure difference and overturning rate is a constant which is invariant under different climate condition.

The school of push views the thermohaline circulation as pressure controlled. Although the school of push may not work for the steady circulation, many people believe that the strong circulation induced by sudden cooling may well be a strong support for this theory. However, as discussed in our previous lectures on energetics of oceanic general circulation, the strong circulation after the onset of sudden cooling is due to the large amount of gravitational potential energy released due to surface cooling. In fact, the total amount of mechanical energy for the mean state is greatly reduced during such sudden cooling. Furthermore, the circulation would die out late, if there was no continuous supply of external source of mechanical energy.

2) School of pull by deep mixing: Deep mixing transforms cold water in the deep ocean into warm water, creating room for newly formed deepwater and thus pulling the thermohaline circulation. The most important argument supporting this case is presented in Munk and Wunsch (1998) and Huang (1999).

3) School of pull by wind stress: Under the present-day climate condition and modern geographic and topographic distribution there is a strong Ekman upwelling around the latitude band of 50-60^{o}S, which is closely related to the Antarctic Circumpolar Current. Due to the strong upwelling in the Southern Ocean, North Atlantic Deep Water (NADW) is pulling up to the upper ocean, where their properties are gradually modified in the surface mixed layer on the way northward. Theoretically, wind-driven upwelling and mixing in the upper ocean can accomplish the major parts of the thermohaline circulation and water mass transformation and the remaining part of the water mass transformation is relatively small.

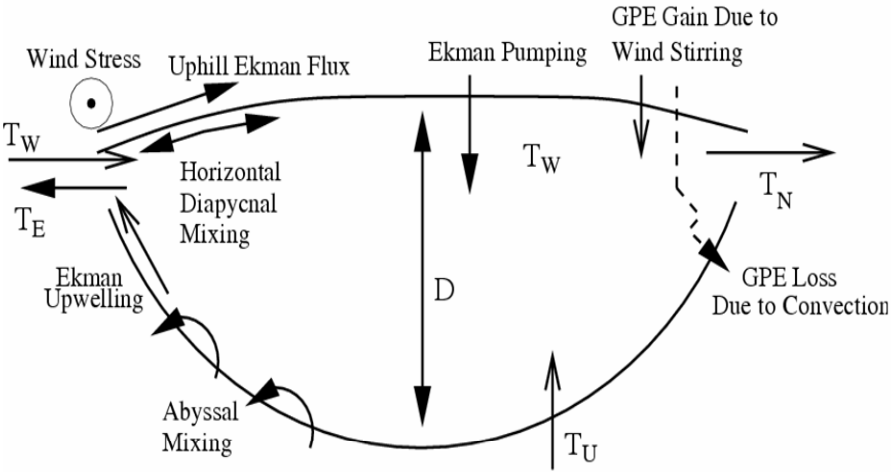

A sketch of different roles of mixing and upwelling in the Atlantic basin.

The basic ideas of this school can be traced back to early works by Toggweiler and Samuel (1995), and it is also consistent with the fact that wind stress energy input to the ocean is much larger than that due to tidal mixing. In addition, this is can be supported by simple scaling based on the formula postulated by Gnanadesikan (1999), as discussed in our previous lectures.

The school of pull views the thermohaline circulation as energy controlled. Of course, the circulation rate is not necessarily linearly proportional to the amount of mechanical energy sustaining the circulation. In comparison, the energy paradigm is relatively young, and it will take long time and effort to be mature and compete with the pressure paradigm.

Note that the circulation system is a very complicated system, thus, we may study the circulation system from quite different angle. For example, one can study the momentum balance of the system, and this is close to the spirit of school of push. One can also study the circulation from mechanical energy balance, and this is the school of pull.

In addition, one may also study the circulation from the balance of entropy of the circulation system. Entropy balance is one of the most important thermodynamic law governing the universe. Examining the thermohaline circulation from the balance of entropy may provide us with some new insight for the circulation; however, this approach has not been pursued, with a few exceptions. A preliminary balance of the entropy in the world ocean can be found in Yan et al. (2004).

2. Thermohaline Circulation based on box models

A. Introduction

Thermohaline circulation is driven by three major driving forces: wind stress, heat flux, freshwater flux. For a long time the same relaxation condition was used for both the temperature and salinity balance in OGCM. Apparently, this is a very "NICE" way to run a model because no matter what model you use, it always gives back the right SST and SSS pattern. Thus, modelers were content with this approach. People did try other types of boundary condition for salinity; however, the model's solutions draft away from the present circulation. It was the sign of multiple solutions for the thermohaline circulation; however, people did not pay much attention to this issue. Thus, although Stommel (1961) wrote about multiple solutions, for more than 20 years nobody took his solutions very seriously.

In the beginning of 1980, the possibility of multiple states in climate and the oceanic circulation became hot issue. Rooth (1982) raised the issues of multiple solutions again. It was said that Rooth went to GFDL and tried to find the multiple solutions, but he could not find them. At that time, F. Bryan was a student in GFDL. After much effort, he was able to find the multiple solutions. In order to find such solutions, he designed a special technique that is still widely used today. His technique will be discussed in the following sections.

Thermohaline circulation in the oceans is controlled by the thermal forcing and fresh water flux through the air-sea interface. Physical processes involved in these two forcing are quite different; however, these differences have not been fully recognized for long time. Traditionally, both the temperature and salinity are treated similarly in the

oceanic circulation models. For example, the same diffusion coefficient is used for both constituents, and the same kind of Rayleigh condition is used as the upper boundary condition for both the temperature and salinity. Furthermore, most physical oceanographers are busy working with the present circulation. Since the oceans are extremely large and the circulation must has potentially a large inertia, a picture of quasi-steady thermohaline circulation appears very naturally to scientists and laymen as well. However, there has been much evidence that the thermohaline circulation does change on time scale of century and thousands of years.

Stommel (1961) first recognized the possibility of multiple solutions of the thermohaline circulation. The sudden change associated with transition from one state of the thermohaline circulation to the other might be associated with catastrophic change in the climate; thus, the thermohaline circulation becomes a hot topic during the past decade.

Note that in this section we will discuss simple models based on the classical conceptions that thermohaline is driven by meridional difference in buoyancy. Over the past 5-8 years, many new model runs based on the energy constraint have been discussed, with some quite exiting new insight; however, this is still a new research frontier, so we will not discuss such results here.

B. Multiple solutions in a 2-box model

Stommel (1961) used a two-box model to illustrate the basic idea: The ocean is idealized as two boxes that are connected by an open channel in the upper level and a pipe on the bottom, Fig. 2.1. The upper channel represents the communication through the ocean interior, and the pipe below is equivalent to the deep western boundary current in the ocean.

a) Two stages of adjustment: the first is temperature controlled (on short time scale), and the second is salinity controlled (on long time scale).

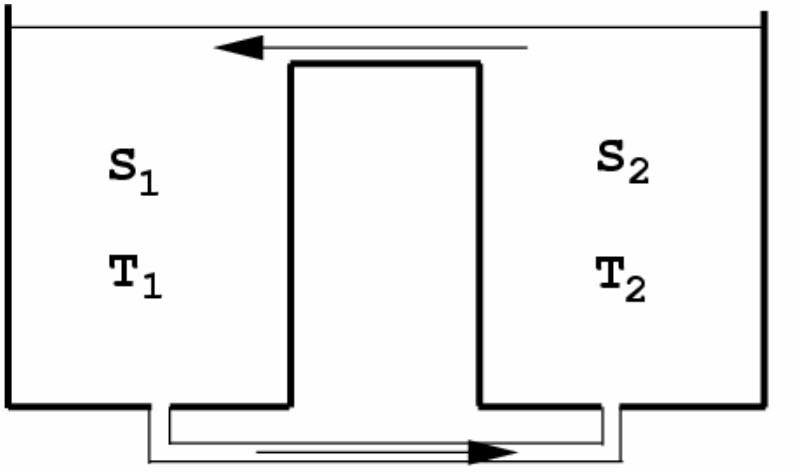

Fig. 3. A two-box model for the thermohaline circulation, Stommel (1961).

b) For given parameters, there are two critical density ratio $R_T >> R_S$.

2) Multiple solutions from the two-box model

Both the temperature and salinity is forced by a relaxation condition,

$$\frac{DT}{dt} = \Gamma_T \left(T^* - T \right), \frac{DS}{Dt} = \Gamma_S \left(S^* - S \right)$$

Although most modeler use $\Gamma_T = \Gamma_S$ even up to now, Stommel realized that the relaxation time for the salinity should much longer than that of the temperature. He pointed out that as a result of this difference in relaxation constant, the first stage of adjustment (on short time scale) is temperature-controlled, and the second stage of adjustment (on long time scale) is salinity-controlled. Most importantly, Stommel demonstrated that if the ratio of these two relaxation times is large than a critical value, there can be three possible steady states under the same forcing, Fig. 2.2. After introducing a pair of new variables the steady states of the model can be found analytically, and the solutions include:

i) A stable state that is thermally controlled, with a relatively fast circulation.
ii) A stable state that is salinity-controlled, with a quite slow circulation. The relatively slow circulation in the haline mode can be explained as follows. Haline mode is dominated by a salinity difference that is large enough to overcome the density difference due to temperature component. Such a large salinity difference is possible for a slow circulation only because the long relaxation time scale.
iii) An unstable state that is thermally controlled.

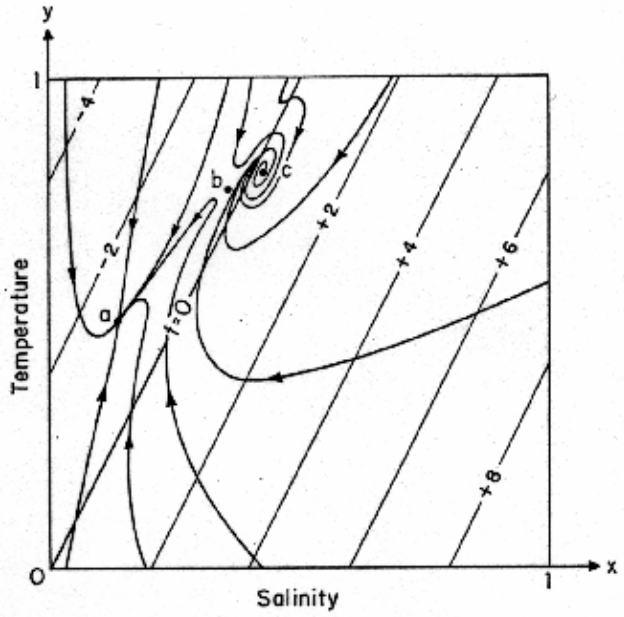

Fig. 4. The three equlibria a, b, and c for the two-box model with R=2, $\delta = 1/6$, $\lambda = 1/5$: the stable note a, the saddle b, and the stable spiral c, Stommel (1961).

C. 3-box model by Rooth (1982)

Stommel's idealized 2-box model remained unnoticed for 20 years. Stommel' original model is formulated for a single hemisphere, i.e., between the equator and high latitudes. Rooth (1982) made the second step by formulating a 3-box model, Fig. 2.3, which consists of one equatorial box and two hemisphere boxes. He noticed that there should be FOUR possible modes in the system. And he suggested that a symmetric solution might be unstable and could drift toward a pole-pole mode.

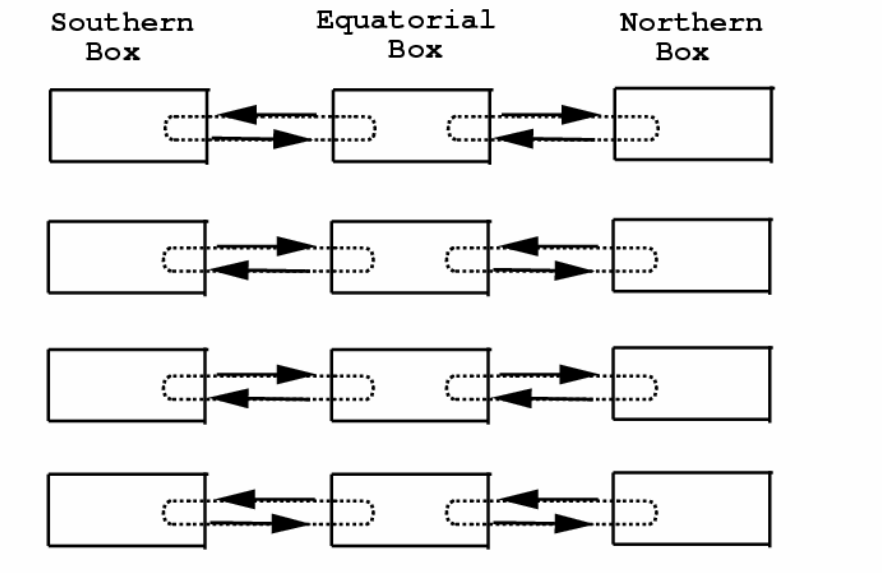

Fig. 5. Three-box model for a two-hemisphere ocean, Rooth (1982).

D. Existing problems:
The relaxation condition for salinity used in the models can be replaced by the natural boundary condition; however, the results is not very sensitive to the choice of the upper boundary condition for the salinity, see Huang et al. (1992).

E. Instability of the symmetric thermal mode (Walin, 1985)
Assuming there is a steady thermohaline circulation which is symmetric with respect to the equator, with sinking at high latitudes due to strong cooling, Fig. 6.

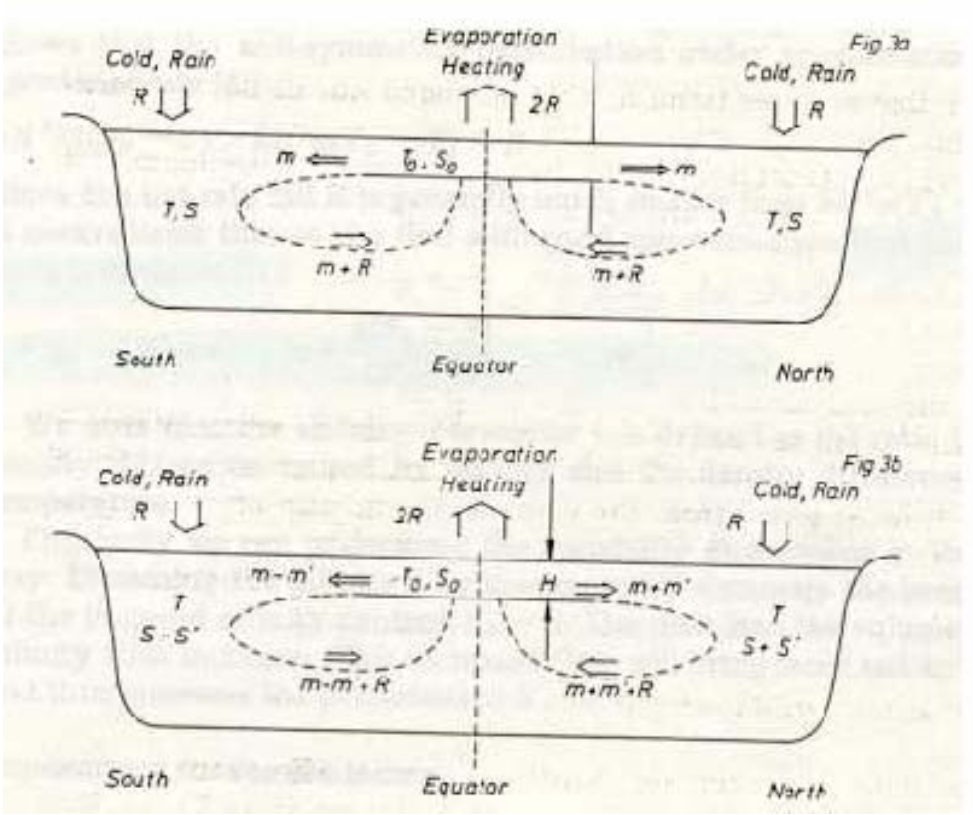

Fig. 6. Thermohaline circulation in two-hemisphere basin. (a) The top layer is warmer and more saline than the deep water. The contrast is counteracting the thermally forced circulation; (b) he asymmetric circulation will grows, if the salinity has sufficient influence on density between the top and deep water, (Walin, 1985).

The basic state can be described in terms of mass flux:

$$m = \kappa H^2 \left[\alpha \left(T_0 - T \right) - \beta \left(S_0 - S \right) \right];$$

Salinity balance:

$$mS_0 - (m+R)S = 0$$

Because the strong temperature relaxation, the temperature perturbation T' is negligible; thus, the salinity perturbation satisfies

$$\frac{\partial S'}{\partial t} > (m+m')S_0 - \left(m+m'+R\right)\left(S+S'\right) > \left\{ \kappa H^2 \left[\alpha (T_0 - T) + 2\beta (S_0 - S) - R \right] \right\} S'$$

If $R_\rho = \dfrac{\alpha (T_0 - T)}{\beta (S_0 - S)} < 2$, a perturbation to the saline component parasitic to the thermal mode is unstable and it will grow. As a result, the system develops in the following way:

1) The thermohaline circulation is asymmetric with respect to the equator, and there is cross-equator flow of the thermohaline circulation. (This is true for both the Atlantic and Pacific)

2) The density ratio, R_ρ, is driven toward the value larger than 2.

Note that Stommel (1993) proposed a salt regulator theory of the oceanic mixed layer. According to his theory, the stochastic forcing by rainstorm, the density ratio in the oceans is driven toward a value of 2.

F. The 2x2 model

a) The model formulation

Assume that properties are uniform within each box, and density is calculated using a linear state equation

$$\rho_i = \rho_0(1-\alpha T_i + \beta S_i),\ i = 1,2,3,4 \qquad (1)$$

The pressure is calculated by the hydrostatic relation. It is assumed that the meridional velocity is proportional to the horizontal pressure gradient

$$u^+ = c\frac{P_1 - P_2}{L},\ u^- = c\frac{P_3 - P_4}{\delta L} \qquad (2)$$

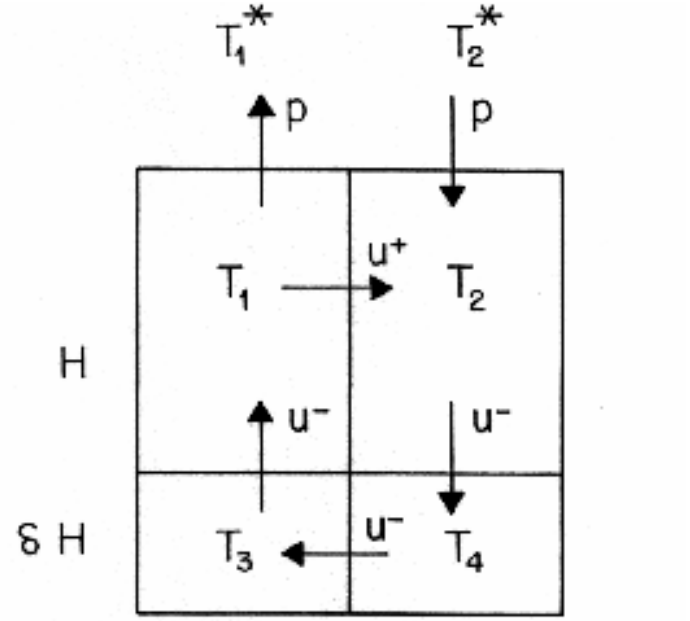

Fig. 7. The 2x2 box model defining applied air temperature T_i^*, amplitude of precipitation p, temperature of boxes T_i, velocities u^+, u^-, box thickness H and δH, and box width L (Huang et al., 1992).

Note that velocity in the lower layer is inversely proportional to the layer thickness, so the total mass flux in the lower layer $\delta H u^-$ remains finite for the case $\delta \to 0$. A finite mass flux associated with a very thin lower layer is a parameterization of the deep western boundary currents observed in the oceans. The pressure horizontal differences in the upper and lower layers are

$$P_1 - P_2 = \Delta P_a + \frac{gH}{2}(\rho_1 - \rho_2)$$

$$P_3 - P_4 = \Delta P_a + gH(\rho_1 - \rho_2) + \frac{g\delta H}{2}(\rho_3 - \rho_4)$$

where ΔP_a is the unknown atmospheric pressure difference, which can be eliminated using the continuity equation

$$u^+ H + pL = u^- \delta H$$

The corresponding velocity expression is

$$u^+ = -\frac{L}{2H} p - \frac{cgH}{4L}\left[\rho_1 - \rho_2 + \delta\left(\rho_3 - \rho_4\right)\right]$$

Introducing the non-dimensional variables $u^+ = \frac{L\Gamma}{H} u^{+'}$, $p = \Gamma p'$, $T = T_0^* T'$, $S = S_0^* S'$, after dropping primes over these new variables this equation is reduced to

$$u^+ = -\frac{p}{2} + \left[A\left(T_1 - T_2 + \delta T_3 - \delta T_4\right) - B\left(S_1 - S_2 + \delta S_3 - \delta S_4\right)\right] \quad (3)$$

where

$$A = C\alpha T_0^*,\ B = C\beta S_0^*,\ C = \frac{cgH^2\rho_0}{4\Gamma L^2} \quad (4)$$

Note that this assumption implies that the circulation is frictionally controlled, and the rotational effect is neglected because it is almost impossible to introduce rotation into such a highly truncated model. It is almost surprise to see that such a frictional model is able to simulate the meridional overturning quite successfully, the success of the model also implies that the meridional circulation is controlled by the frictional processes within the western boundary currents.

The upper boundary condition for the temperature is a Rayleigh condition

$$H_f = \rho_0 c_p \Gamma\left(T^* - T\right) \quad (5)$$

The upper boundary condition for the salinity is a flux of plain water specified at each upper-layer box. The algebraic sum of the applied fresh water fluxes is zero.

The non-dimensional equations for the heat and salt balance in the upper boxes are

$$\frac{dT_1}{dt} = -u^+ T_1 + u^- T_3 + 1 - T_1 \quad (6)$$

$$\frac{dT_2}{dt} = u^+ T_1 - u^- T_2 - T_2 \quad (7)$$

$$\frac{dS_1}{dt} = -u^+ S_1 + u^- S_3 \quad (8)$$

$$\frac{dS_2}{dt} = u^+ S_1 - u^- S_2 \quad (9)$$

The equations for the lower boxes are

$$\frac{dT_3}{dt} = \frac{u^-}{\delta}\left(T_4 - T_3\right) \quad (10)$$

$$\frac{dT_4}{dt} = \frac{u^-}{\delta}\left(T_2 - T_4\right) \quad (11)$$

$$\frac{dS_3}{dt} = \frac{u^-}{\delta}\left(S_4 - S_3\right) \quad (12)$$

$$\frac{dS_4}{dt} = \frac{u^-}{\delta}(S_2 - S_4) \quad (13)$$

where the velocity satisfies the continutity equation

$$u^- = u^+ + p \quad (14)$$

These equations are based on the so-called upwind scheme, and they are valid for the circulation pattern indicated in Fig. 3.1 only. If the circulation reverses sign, the corresponding equations are slightly different, and the reader can derive them accordingly. According to Haney (1971), $\frac{\Gamma}{\rho_0 c_p} = 8.1\times10^{-4} cm/s$. The parameter C=0.05 is chosen to give a vertical velocity comparable to observations, the evaporation/precipitation index p is about $0.38\times10^{-5} cm/s$.

There are three types of mixing in the model. First, properties carried by advection into each box are homogenized within each box. Second, there is numerical mixing due to the upwind scheme. Third, there is mixing associated with convective overturning, the so-called convective adjustment in many numerical model. Essentially, gravitationally unstable situation may occur due to cooling at the surface, and water within the unstable column will mix vertically till a stable stratification is obtained. However, there is no other source of mixing.

b) Reduction to a 2-box model

As $\delta \to 0$, the model is reduced to the classic 2-box model by Stommel (1961), with a minor difference because the different upper boundary condition for the salinity. Essentially, box 3 and 4 shrink and become a "pipe" linking box 1 and 2. Note that the pipe is a beautiful idealization of the deep western boundary current in the world oceans. For case of $u^+ > 0$

$$T_3 = T_4 = T_2,\ S_3 = S_4 = S_2 \quad (15)$$

Therefore, the equations are reduced to

$$\frac{dT_1}{dt} = -u^+T_1 + u^-T_2 + 1 - T_1 \quad (16)$$

$$\frac{dT_2}{dt} = u^+T_1 - u^-T_2 - T_2 \quad (17)$$

$$\frac{dS_1}{dt} = -u^+S_1 + u^-S_2 \quad (18)$$

$$\frac{dS_2}{dt} = u^+S_1 - u^-S_2 \quad (19)$$

The velocities are

$$u^+ = -\frac{p}{2} + C(T - S),\ u^- = u^+ + p \quad (20)$$

where

$$T = \alpha T_0(T_1 - T_2),\ S = \beta S_0(S_1 - S_2) \quad (21)$$

There are three zones in the (S, T) phase space: region I where $u^+ \geq 0$, $u^- \geq 0$; region II where $u^+ < 0$, $u^- \leq 0$; region III where $u^+u^- < 0$. However, region III is unphysical

because salt would be wiped out from half of the model basin, if both velocities are in the same direction.

Now we look for the steady states that can be characterized by

Heat equilibrium curve within region I and II:

$$S = \frac{1}{2C} + T - \frac{1+p}{2C}\frac{T_0}{T} \qquad \text{Region (I)}$$

$$S = -\frac{1}{2C} + T + \frac{1+p}{2C}\frac{T_0}{T} \qquad \text{Region (II)}$$

Salt equilibrium curve within region I and II:

$$T = S + \frac{pS_0}{CS} \qquad \text{Regime} \qquad \text{(I)}$$

$$T = S - \frac{pS_0}{CS} \qquad \text{Region} \qquad \text{(II)}$$

The intersections of these two curves are solutions are steady solutions for the model, Fig. 8. When $p\langle pc\rangle$ there are three solutions, one stable solution and on unstable solution belong to the thermal mode and one haline mode solution. As $p \to p_c$, the two thermal mode solutions coalesce and this is the critical situation where the "catastrophe" would occur, if p is slightly increased. When p is larger than p_c, there is only the haline mode.

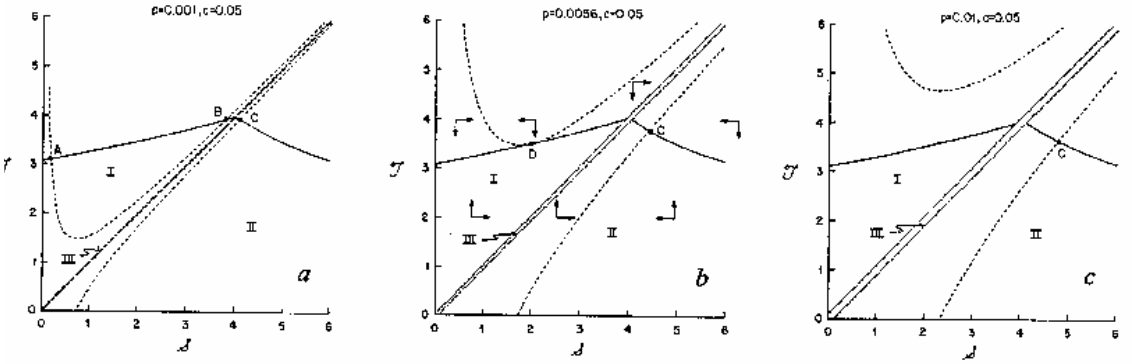

Fig. 8. S-T phase diagram for the 2x1 box ($\delta \to 0$). The panels are for different values of p (nondimensional). The phase space consists of three regions: I, II, and III, characterizing different velocity pattern. The curve for heat equilibrium is solid; that for salt equilibrium is dashed. Intersections of these two sets of curves define equilibrium states. The intersection at point A is a stable thermally driven equilibrium. Point B is unstable. Point C is a stable salinity-dominated equilibrium. Point D represents the coalescence of points A and B at the critical $p_c = 0.0056$. In Panel (b) there are pairs of arrows to show the directions of S_i and T_i in region bounded by the equilibrium curves (Huang et al., 1992).

By definition, in a thermal mode the flow is temperature-controlled, that means a poleward flow in the upper layer which is relatively fast; a haline mode is salt-controlled, that means an equatorward flow in the upper layer which is relatively slow.

c) Transition from a thermal mode to a saline mode

If p is close to the critical value p_c, a small increase in p would induce a catastrophic transition from the thermal mode to the haline mode. The transition consists of three stages: 1) a searching stage, 2) a catastrophic stage, and 3) an adjustment stage during which the deep boxes adjust their temperature and salinity to the new equilibrium values, Fig. 9.

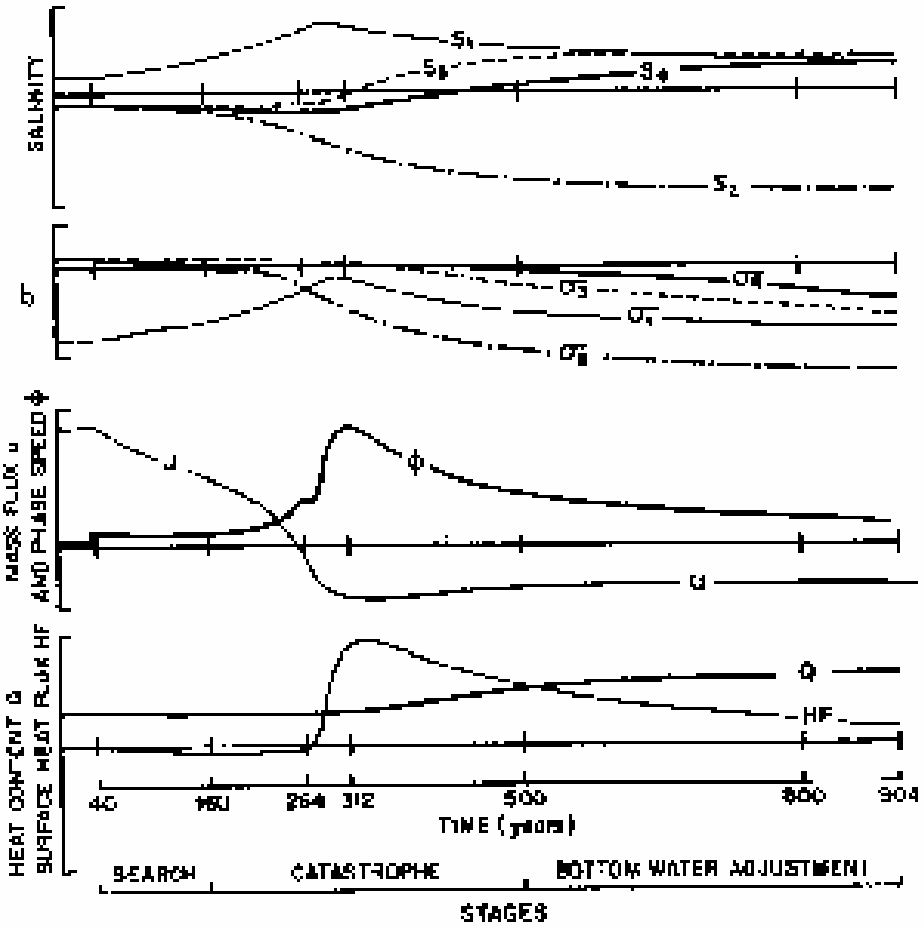

Fig. 9. Evolution of the 2x2 ($\delta = 1$) system from thermally driven equilibrium state to a salinity-driven equilibrium state, as caused by a discrete increase of p at time year 40, so that p exceeds the critical value. The evolution passes through three stages (Huang et al., 1992).

The system exhibits a hysteric behavior as the strength of evaporation minus precipitation gradually increase and decrease, Fig. 10. As the precipitation increases, the system remains in the thermal mode with the meridional circulation decreases gradually. As p approaches p_c, the system can no longer remain in the thermal mode; however, there is a forbidden region, so the transition from the thermal mode to the haline mode must be catastrophic.

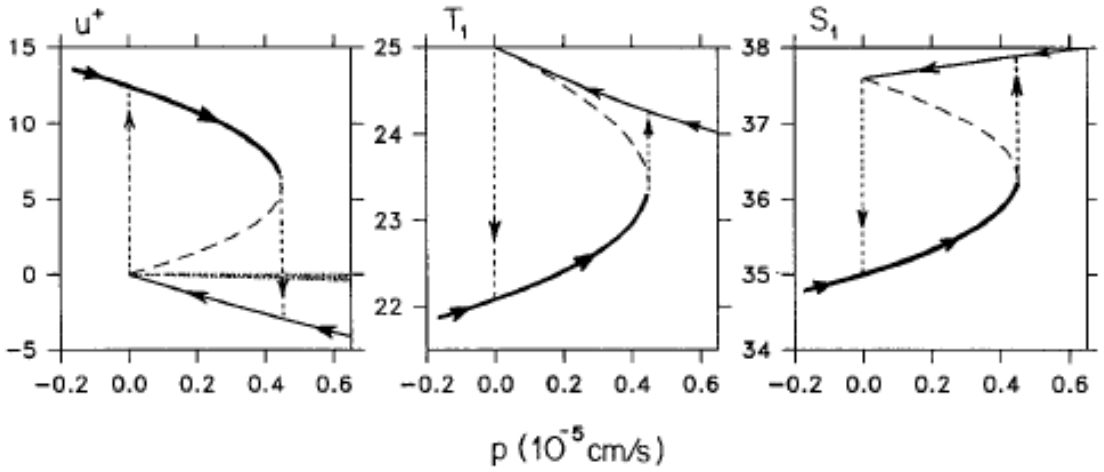

Fig. 10. Dependence of the equilibrium values of u^+ (in units of $10^{-5} cm/s$), T_1 and S_1 upon p, for the 2x2 ($\delta = 1$) box model. Heavy solid curve for p increasing by small increments, thin solid curve for p decreasing (thus illustrating the hysterics of the system), long-dashed lines for an unstable state. The short-dashed lines indicate abrupt transitions, (Huang et al., 1992).

The essential ingredient for thermohaline catastrophe is the difference in upper boundary conditions for the temperature and salinity; that is a large Rayleigh coefficient (Stommel, 1961) or a flux condition for the salinity (the present case).

d) Monte Carlo experiments

Since the system has multiple solutions, one way to study the size of the basin of attraction is to run the Monte Carlo experiments. For a given p, the model is integrated from initial state of random temperatures in each box, between o^oC and 25^oC and random salinity between 31.5 and 38.5. The probability of ending up in either of the two stable modes is shown in Fig. 11. According to the model's results, the thermohaline circulation in the North Atlantic is close to a critical state, and small increase in the precipitation can cause a catastrophic transition from the current thermal mode to the haline mode.

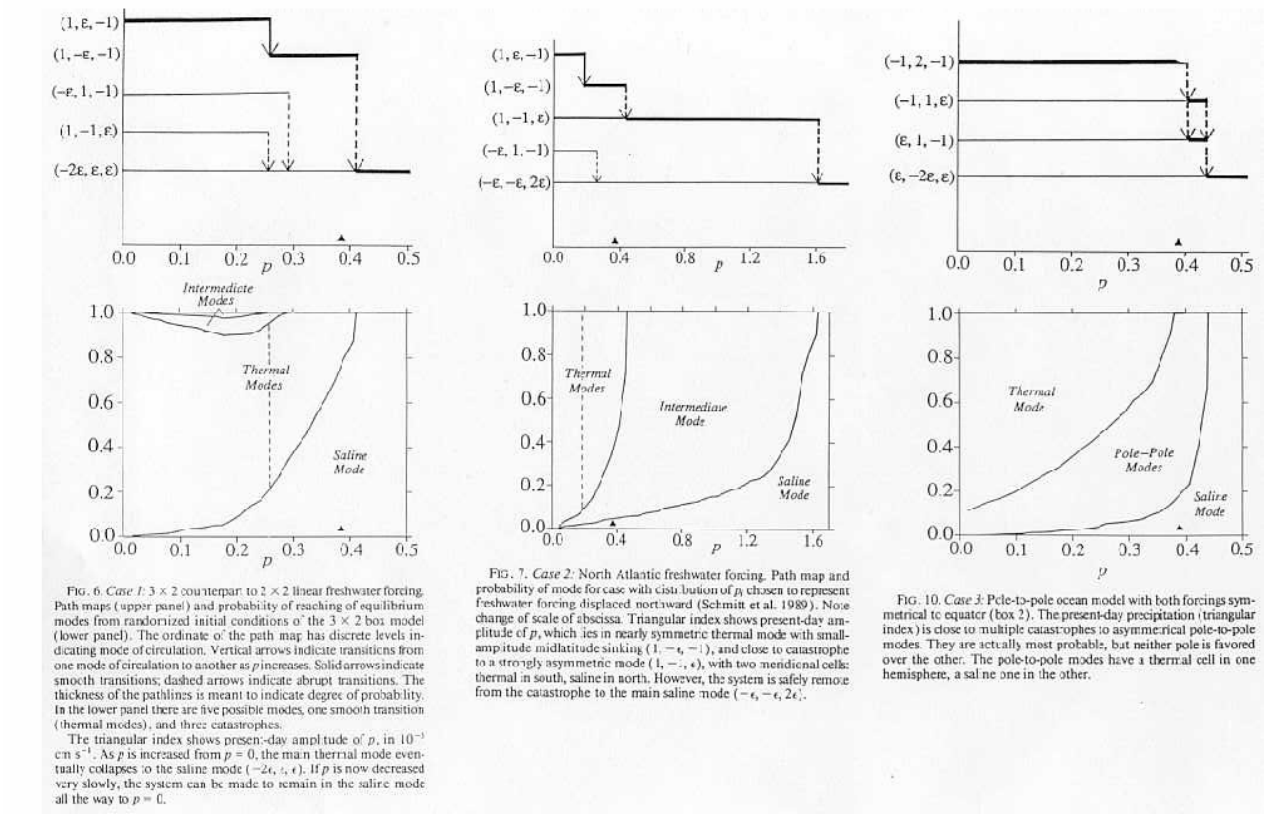

FIG. 6. *Case 1:* 3 × 2 counterpart to 2 × 2 linear freshwater forcing. Path maps (upper panel) and probability of reaching of equilibrium modes from randomized initial conditions of the 3 × 2 box model (lower panel). The ordinate of the path map has discrete levels indicating mode of circulation. Vertical arrows indicate transitions from one mode of circulation to another as p increases. Solid arrows indicate smooth transitions; dashed arrows indicate abrupt transitions. The thickness of the pathlines is meant to indicate degree of probability. In the lower panel there are five possible modes, one smooth transition (thermal modes), and three catastrophes.

The triangular index shows present-day amplitude of p, in 10^{-3} cm s^{-1}. As p is increased from $p = 0$, the main thermal mode eventually collapses to the saline mode $(-2\epsilon, \epsilon, \epsilon)$. If p is now decreased very slowly, the system can be made to remain in the saline mode all the way to $p = 0$.

FIG. 7. *Case 2:* North Atlantic freshwater forcing. Path map and probability of mode for case with distribution of p_3 chosen to represent freshwater forcing displaced northward (Schmitt et al. 1989). Note change of scale of abscissa. Triangular index shows present-day amplitude of p, which lies in nearly symmetric thermal mode with small-amplitude midlatitude sinking $(1, -\epsilon, -1)$, and close to catastrophe to a strongly asymmetric mode $(1, -\epsilon, \epsilon)$, with two meridional cells: thermal in south, saline in north. However, the system is safely remote from the catastrophe to the main saline mode $(-\epsilon, -\epsilon, 2\epsilon)$.

FIG. 10. *Case 3:* Pole-to-pole ocean model with both forcings symmetrical to equator (box 2). The present-day precipitation (triangular index) is close to multiple catastrophes to asymmetrical pole-to-pole modes. They are actually most probable, but neither pole is favored over the other. The pole-to-pole modes have a thermal cell in one hemisphere, a saline one in the other.

Fig. 11. Monte Carlo experiments for the box model, including the probability of each equilibrium states. a) A 3x2 box model; b) A model for the North Atlantic; c) A pole-pole model.

The Monte Carlo experiments carried out for a 3x2 model, with a linear profile of evaporation minus precipitation, demonstrates that there are grand modes that are the mostly probable modes. Although there are many possible modes, most of them have very small probability and is very unlikely to appear, Fig. 11.

A 3x2 model forced by observed evaporation minus precipitation shows that for the current level of evaporation minus precipitation the most likely mode is an intermediate mode which is characterized by sinking at the mid-latitude box, Fig. 11a. The intermediate mode may have some connection with the intensification of the intermediate water formation existed during the last glaciations.

3. Loop oscillators for the thermohaline circulation

A. The system can be formulated under two slightly different boundary conditions: the natural boundary condition and the virtual salt flux condition. The model based on the virtual salt flux condition can be reduced to an ordinary differential equation system, the water wheel equation. Water wheel experiments were first carried out by Malkus and Howard in MIT in 1970s (Malkus, 1972). The experiment set-up is relatively simple, as shown in the following figures.

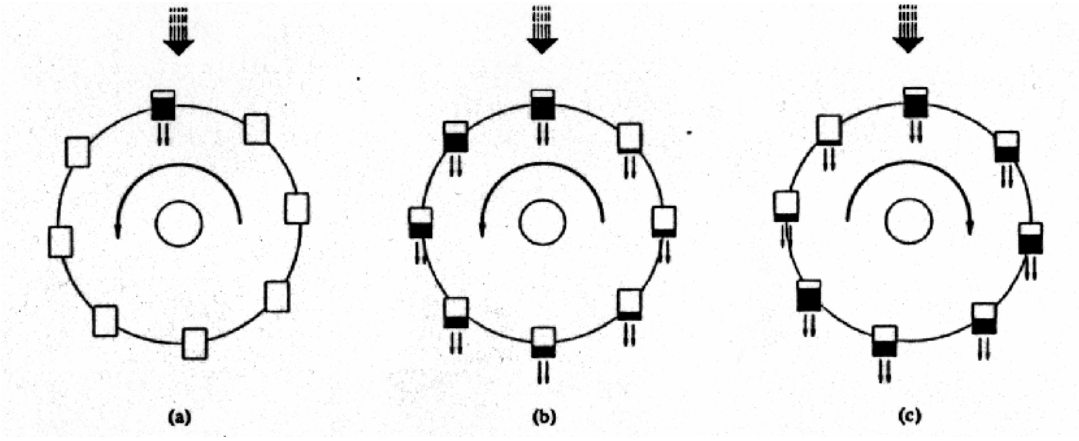

Fig. 12. Sketch of the water wheel designed by Willem Malkus and Lou However at MIT in the 1970s. The simplest version is a toy waterwheel with leaky paper cups suspended from its rim.

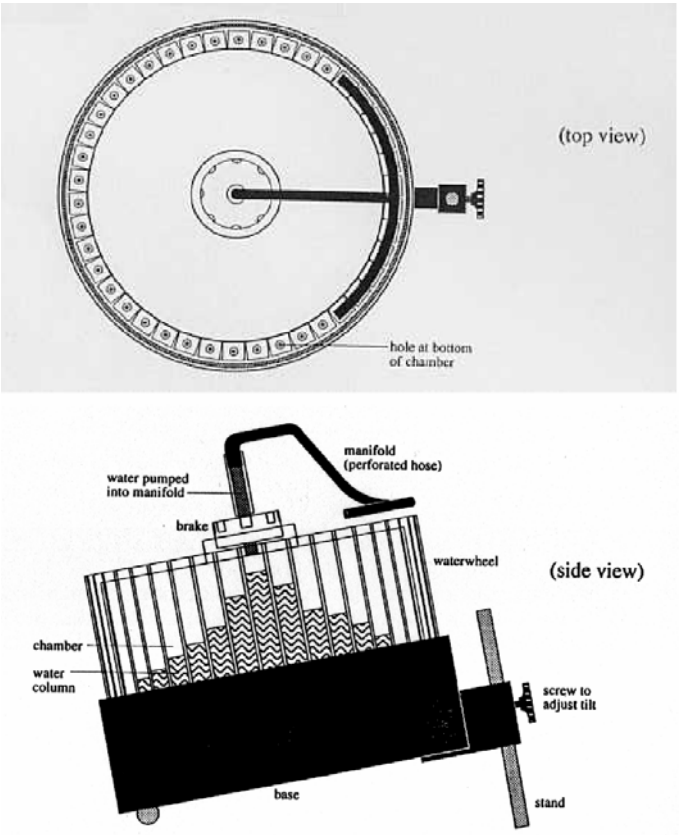

Fig. 13. A more sophisticated water wheel model.

When water flow rate is too slow, the top cups are not filled up enough to overcome the friction (note that cups are leaky), so the wheel remains motionless due to friction. When flow rate is large enough, the wheel starts to rotate, and the rotation is in a steady state in either direction. When the flow rate is large enough, the motion become chaotic.

B. A loop model forced by evaporation and precipitation

The thermohaline circulation in the oceans can have regular or irregular oscillations over a wide spectrum. One of the simplest ways to study such phenomena is to use the so-called loop models, Fig. 12. Loop models have been studies extensively in many fields, including many engineering application, so you can find a lot of good papers to read. For the thermohaline application, you may read Huang and Dewar (1996, JPO).

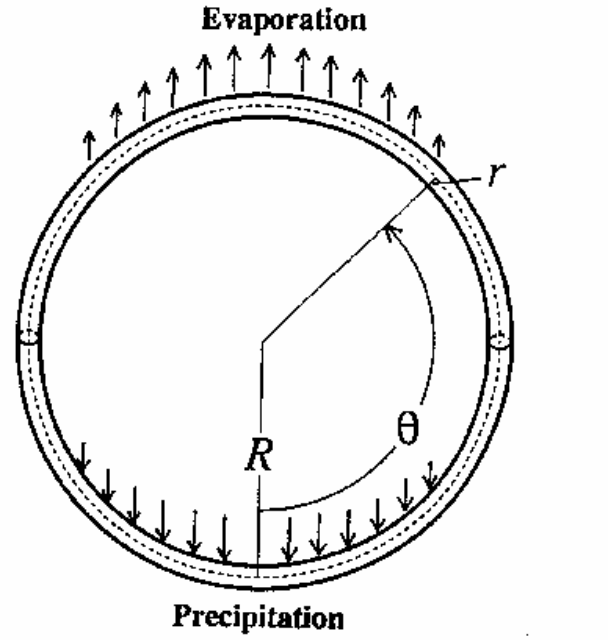

Fig. 14. A loop oscillator for the haline circulation -- a tube filled with salty water. The fresh water is passed through the skin of the tube, Huang and Dewar (1996)

a) Model Formulation

The model consists of a loop filled with salty water (see Fig. 14). The radius of the loop is R and the radius of the tube is r. In the following analysis, we will assume that $R \gg r$, and that the flow and water properties are uniform in each cross section. At the surface of the tube, freshwater is exchanged with the environment in the form of precipitation (p) and evaporation (e):

$$p - e = E\cos\theta \tag{22}$$

(1) Continuity.

Under the Boussinesq approximation, continuity requires that the velocity convergence equal the freshwater flux

$$u_\theta = 2RE\cos\theta / r \tag{23}$$

In the following analysis, we use angular velocity, defined as

$$u = R\omega \tag{24}$$

Thus, integrating (23), we obtain

$$\omega = \Omega + 2E\sin\theta / r \tag{25}$$

where Ω is the mean angular velocity of the water circulating the loop, and the second term on the right-hand side is due to the accumulated water caused by the freshwater flux through the surface of the tube.

(2) Salt Conservation.

Similarly, the salt conservation equation is

$$S_t + (\omega S)_\theta = KS_{\theta\theta} / R^2 \tag{26}$$

where *K* is the coefficient of salt diffusivity. For comparison, the salt conservation equations subject to virtual salt flux and relaxation boundary conditions are

$$S_t + (\Omega S)_\theta = \frac{-2E}{r}\overline{S}\cos\theta + \frac{K}{R^2}S_{\theta\theta} \tag{27}$$

$$S_t + (\Omega S)_\theta = \frac{2\Gamma}{r}\left(S^* - S\right) + \frac{K}{R^2}S_{\theta\theta} \tag{28}$$

where Γ is a relaxation coefficient, $\overline{S}$ an average salinity and S^* a specified reference salinity (traditionally chosen to be the observed salinity). Note that the net salt in the problem is guaranteed to be a constant if Eqs. (26) or (27) are used. No such guarantee exists for (28).

(3) Momentum Equation

The momentum balance for an infinitely small sector of water is

$$\rho_0\left(u_t + uu_l\right) = -P_l - \rho g\sin\theta - \varepsilon\rho_0 u \tag{29}$$

where *l* is the arc element along the axis of the tube, P_l is the pressure gradient, ε is the frictional coefficient. Integrating (29) around entire loop, we obtain

$$\Omega_t = -\varepsilon\Omega - \frac{g}{2\pi R}\int_0^{2\pi}\frac{\rho}{\rho_0}\sin\theta d\theta \tag{30}$$

In this study we apply a linear equation of state

$$\rho = \rho_0\left(1 + \beta S\right) \tag{31}$$

Thus, (2.7) can be written as

$$\Omega_t = -\varepsilon\Omega - \frac{g\beta}{R}\langle S\sin\theta\rangle \tag{32}$$

where $\langle\ \rangle = \frac{1}{2\pi}\int_0^{2\pi}\cdot d\theta$ is an averaging operator.

(4) Non-dimensionalization.

Eqs. (26) and (32) are non-dimensionalized using

$$S = \overline{S}S', t = Tt', \omega = \omega'/T \tag{33}$$

where

$$T = \sqrt{R/g\beta\overline{S}} \tag{34}$$

After dropping the primes, we obtain

$$\Omega_t = -\alpha\Omega - \langle\sin\theta\rangle \tag{35a}$$

$$S_t + \left[\left(\Omega + \lambda\sin\theta\right)S\right]_\theta = \kappa S_{\theta\theta} \tag{35b}$$

where

$$\alpha = \varepsilon T = \varepsilon\left(\frac{R}{g\beta\overline{S}}\right)^{1/2}, \lambda = \frac{2ET}{r} = \frac{2E}{r}\left(\frac{R}{g\beta\overline{S}}\right)^{1/2}, \kappa = \frac{KT}{R^2} = \frac{K}{R}\left(\frac{1}{gR\beta\overline{S}}\right)^{1/2} \quad (36)$$

are the non-dimensional parameters of the model. The interpretation of T in (34) is as a loop "flushing" time, as determined by buoyancy anomalies; thus, α represents the ratio of flushing time to viscous decay time, λ the ratio of flushing time to a tube "filling" time (due to freshwater flux) and κ the ratio of flushing time to salt diffusion time. In view of these interpretations, one sees we are interested in the limit of small α, λ and κ. Note that (35b) implies a normalization condition for *S*, i.e., $\int_0^{2\pi} S d\theta = 2\pi$.

b. System Behavior

We now consider the solutions of the coupled nonlinear, integro-differential equation set (35). Clearly, numerical methods can provide solutions of the above set for any initial conditions and parameter values. In view of this, we have developed a model which uses a Fourier spectral approach to solve the salt equation. Time stepping for both equations is performed using a fourth-order Runge-Kutta algorithm. An advantage of the spectral technique is that the torque in the momentum equation appears naturally as the coefficient of the lowest Fourier mode. Our interest in the above simple model comes from a desire to understand the oscillations of more complicated climate models; hence, we tend to focus on steady solutions and limit cycle oscillations. Information about these can also be obtained analytically. In the following discussion, we will combine analytical and numerical approaches to demonstrate the expected behavior of the system.

It is perhaps not surprising that the nature of the stationary solutions depends critically on the relative importance of the parameters α, λ and κ.

When $\kappa = 0$, it is straightforward to find the steady solution of (35); i.e. for arbitrary α and λ.

$$S = \left(1 - \lambda/\Omega\right)^{1/2}\left(1 + \lambda\sin\theta/\Omega\right)^{-1} \quad (37a)$$

where

$$\Omega = \pm\sqrt{\frac{\lambda}{\alpha\left(2 - \alpha\lambda\right)}} \quad (37b)$$

is the mean angular velocity.

It is, however, much more interesting to consider non-zero κ because diffusion exists in reality and is also necessary for numerical stability. Also, it should be clear from the preceding section that the regime of most physical interest involves small α and λ, and we shall exploit this by assuming $\alpha \sim \lambda << 1$. When κ is non-zero, the solutions for Ω and *S* can be simply obtained by employing a perturbation approach which makes use of these parametric restrictions. Indeed, a convenient classification of the solutions to (35) is found if we consider κ larger than, comparable to, and smaller than α and λ, respectively. We shall now describe this classification.

The basic equation for the model under the virtual salt flux condition can be reduced to a simple set of ordinary differential equation, the water wheel equation (For the details, please check out the paper by Huang and Dewar):

$$\dot{x} = \alpha(y - x)$$
$$\dot{y} = rx - ky - xz$$
$$\dot{z} = xy - kz$$

This system is very similar to the well-known Lorenz equation:

$\dot{x} = \alpha(y - x)$

$\dot{y} = rx - y - xz$

$\dot{z} = xy - bz$

If $\kappa = 1$, the water wheel equation and the VSF loop model under the present simple forcing are equivalent to the Lorenz system with b=1. The model's behavior is rather complicated and it looks very similar to the behavior of the well-known Lorenz's model, Fig. 15 and 16.

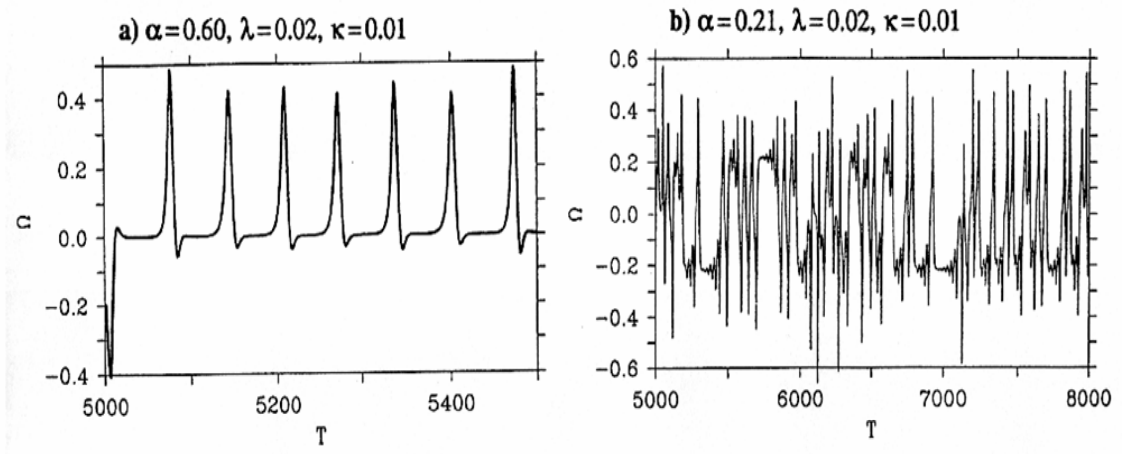

Fig. 15. Chaotic solutions for the model under the natural boundary conditions, Huang and Dewar (1996).

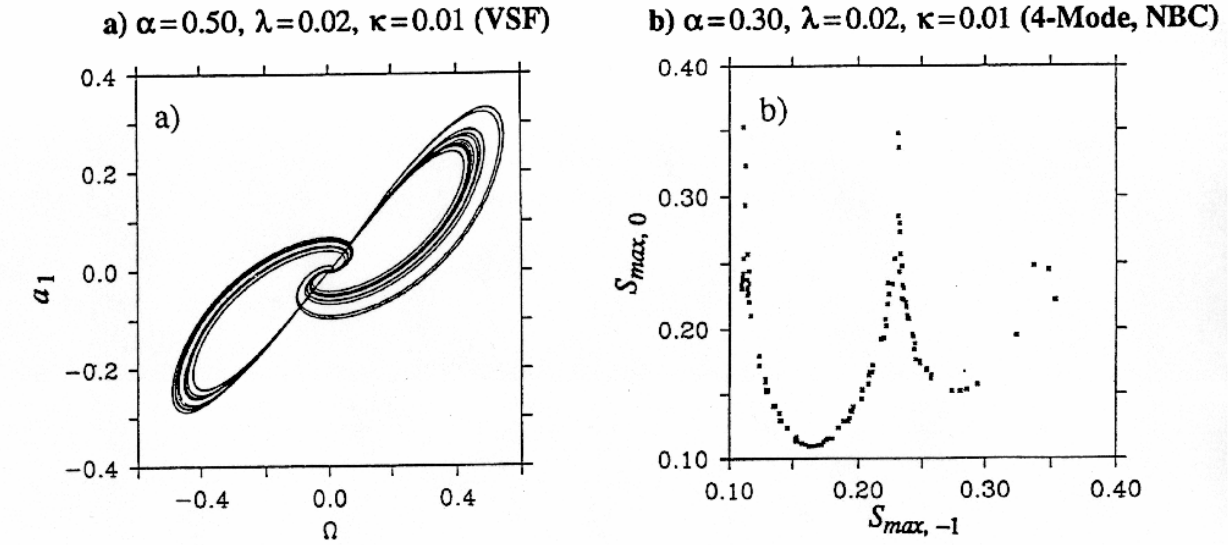

Fig. 16. Butterfly map, amplitude of the $\sin\theta$ mode a_1 vs angular velocity ω, generated from the 2-mode model; b) return map for the 4-mode natural boundary condition, Huang and Dewar (1996).

4. Two-box ice-ocean coupled model

Ice-ocean coupled system can also have multiple solutions, and this can be explained by the simple two-box ice-ocean coupled model by Welander (1977).

A. Model formulation

The model consists of one box filled with homogenized water, Fig. 17.

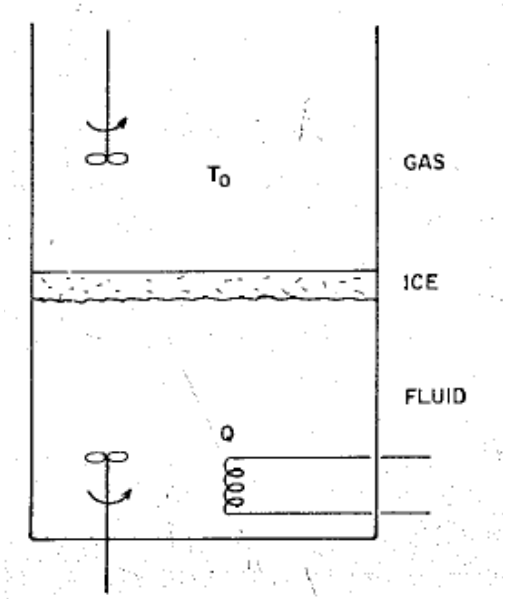

Fig. 17. Sketch of the ice-water coupled system. The fluid is heated at a constant rate Q, while the temperature in the reservoir is kept at a constant low value T_0, allowing freezing at the top (Welander, 1977).

For simplicity, we will neglect the heat content of the ice, but the latent heat associated with ice melting/freezing must be included. The heat flux across the thin boundary layers on both sides of the ice sheet can be parameterized in terms of the temperature difference Fig. 18.

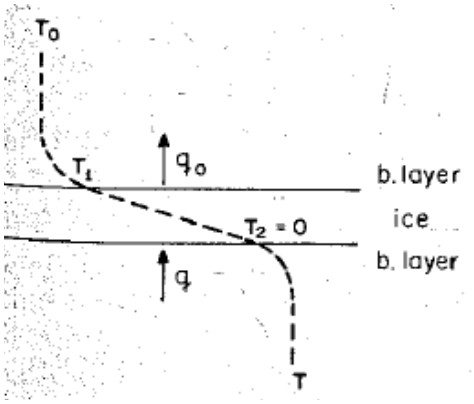

Fig. 18. Temperature profile through the ice-water system. Heat flux is assumed to be proportional to the temperature difference. Deference in heat flux is used for milting the ice. (Welander, 1977).

For the upper surface we have

$$q_0 = k_0\left(T_1 - T_0\right) = K_i\left(T_2 - T_1\right)/\delta \tag{38}$$

Note that ice melting/freezing takes place at the lower surface; thus, the heat flux through the ice sheet should be the same as the heat flux through the upper boundary layer. For the lower surface we have

$$q = k\left(T - T_2\right) \tag{39}$$

In these equations T_2 is the fixed melting temperature, which is set to $T_2 = 0$. The difference between q_0 and Q is the heat for ice melting/freezing, so

$$\rho_i L\dot{\delta} = q_0 - q \tag{40}$$

where ρ_i is the ice density, L is the latent heat for ice melting. The fluid temperature follows

$$\rho cD\dot{T} = Q - q \tag{41}$$

where c is the specific heat, D is the depth of the fluid. Since the depth does not change much, D will be treated as a constant.

From (38), we can solve for T_1

$$T_1 = \frac{\delta k_0 T_0}{\delta k_0 + K_i} \tag{42}$$

Using Eqs. (38) and (39), Eqs. (40) and (41) can be rewritten as

$$\rho_i L\dot{\delta} = -\frac{K_i k_0 T_0}{\delta k_0 + K_i} - kT \tag{43}$$

$$\rho cD\dot{T} = Q - kT \tag{44}$$

Note that these equations apply to the case with ice covering. For the ice-free case, the corresponding equations are

$$\dot{\delta} = 0, \rho cD\dot{T} = Q - k_0^{'}\left(T - T_0\right) \tag{45}$$

where $k_0^{'}$ is the relaxation constant for ice-free air-water interface.

Introducing the non-dimensional variables

$$t = \left(\frac{\rho cD}{k}\right)\cdot t', \delta = \left(\frac{\rho cDQ}{\rho_i Lk}\right)\cdot\delta, T = \left(\frac{Q}{k}\right)\cdot T'$$

the new non-dimensional equations, after dropping the primes, are

$$\dot{\delta} = \frac{a}{\delta + b} - T, \dot{T} = 1 - T, \left(\delta > 0, or\, \delta = 0, T < 0\right) \quad \text{(With Ice)} \tag{46}$$

$$\dot{\delta} = 0, \dot{T} = 1 - c\left(T - \bar{T}\right), \left(\delta = 0, T \geq 0\right) \quad \text{(Ice free)} \tag{47}$$

with the non-dimensional coefficients

$$a = -\left(\frac{\rho_i LkK_i}{\rho ck_0 DQ}\right)\cdot\frac{k_0 T_0}{Q} > 0, b = \frac{\rho_i LkK_i}{\rho ck_0 DQ}, c = \frac{k_0^{'}}{k}, \bar{T} = \frac{kT_0}{Q} < 0 \tag{48}$$

B. Steady state solutions

Steady solutions can be found by setting the right-hand side of (46) and (47) equal to zero. There are possibly two steady solutions:

1) The ice-covered solution:

$$S_0 : T = 1, \delta = a - b \tag{49}$$

2) The ice-free solution:

$$S_1 : T = 1/c + \bar{T}, \delta = 0 \tag{50}$$

There are four possible combinations, shown in Fig. 19.

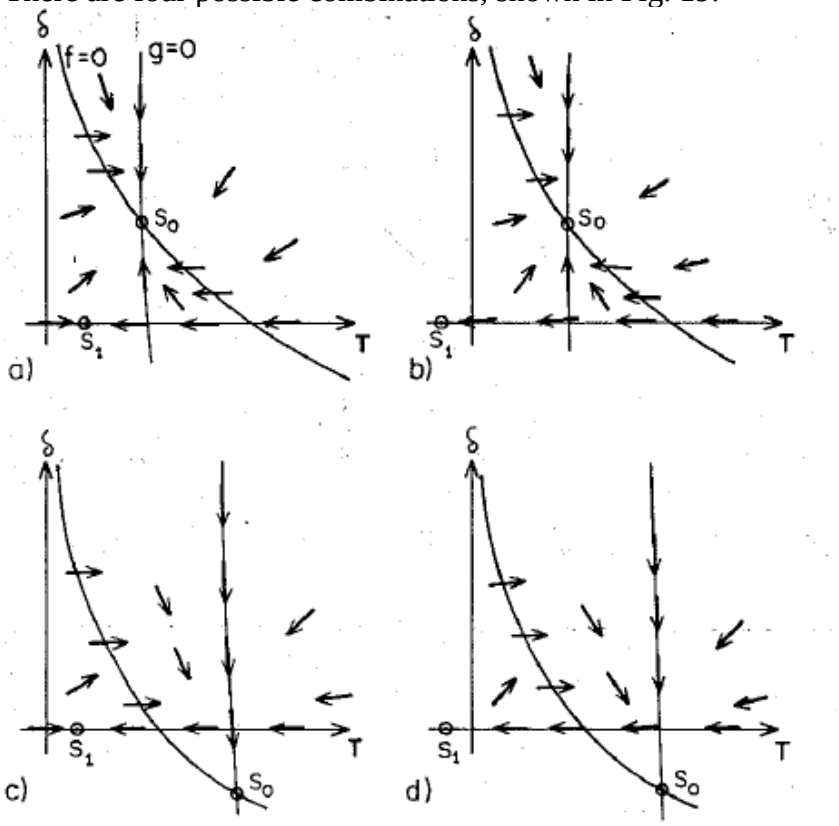

Fig. 19. Schematic pictures of curves $\dot{\delta} = 0$ and $\dot{T} = 0$ (f=0 and g=0) in the T-δ plane, and the direction field for the trajectories. There are two steady states, one with ice (S_0) and one without ice (S_1). The field makes a jump going from $\delta = 0$ to a slightly positive value, or going along $\delta = 0$ from T=0 to a slightly negative T value, making the transition from an ice-free to an ice-covered state. A) Both steady states exist physically (lie in the positive quadrant). B) The ice-free steady state does not exist. C) The ice-covered steady state does not exist. D) both steady states do not exist. (Welander, 1977).

For the first three cases, there is at least one stable node, and the system will eventually fall into such a solution. For the fourth case, these two steady solutions are non-physical. As a result, the system cannot reach a steady solution, instead the system oscillates between the ice-free and ice-covered states,

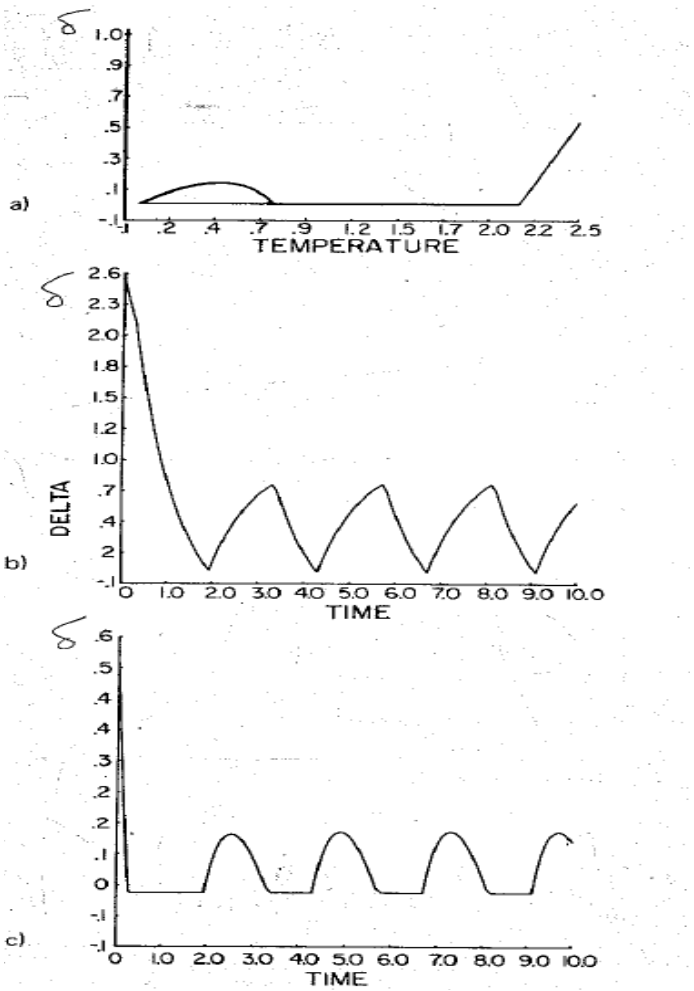

Fig. 20. Examples of a trajectory when no physical steady state exists, corresponding to the case shown in Fig. 3d (a=0.5,b=1.0,c=1.0, $\overline{T} = -1.5$). All trajectories run into the limit cycle shown to the left in panel a. Panel b and c show $\overline{T}$ *and* δ as functions of time for one trajectory. The system oscillates forever between an ice-free and an ice-covered regime. (Welander, 1977).

Reference:

Gnanadesikan, Anand, 1999. A simple predictive model for the structure of the oceanic pycnocline. *Science*, **283**, 2077-2079.

Haney, R. L., 1971: Surface thermal boundary condition for ocean circulation models. J. Phys. Oceanogr., 1, 241-248.

Huang, R. X. and W. K. Dewar, 1996. Haline circulation in a loop model: bifurcation and chaos. *J. Phys. Oceanogr*., **26**, 2093-2106.

Huang, R. X., J. M. Luyten, and H. M. Stommel, 1992. Multiple equilibrium states in combined thermal and saline circulation. *J. Phys. Oceanog*., **22**(3), 231--246.

Malkus, W. R., 1972: Nonperiodic convection at high and low Prandtl number. Mem. Soc. R. Sci. Liege, 6^{e} Ser., IV, 125-128.

Munk, W. H., 1966: Abyssal recipes. *Deep-Sea Res*., **13**, 707-730.

Rooth, C., 1982: Hydrology and ocean circulation. *Prog. Oceanogr.*, **11**, 131-149.

Stommel, H. M., 1961: Thermohaline convection with two stable regimes of flow. *Tellus*, **13**, 224-230.

Stommel, H. M., 1993. A conjectural regulating mechanism for determining the thermohaline structure of the oceanic mixed layer. *J. Phys. Oceanogr*., 23, 142-148.

Walin, G., 1985: The thermohaline circulation and the control of ice ages. *Palaeogeogr., Palaeoclimatol, Palaeoecol*., **50**, 323-332.

Welander, P, 1977: Thermal oscillations in a fluid heated from below and cooled to freezing from above, *Dyn. of Atmos. and Oceans*, **1**, 215-223.

Wytki, K., 1961: The thermohaline circulation in relation to the general circulation in the oceans. *Deep-Sea Res*., **8**, 39-64.

Yan, Y.F., Z.-J. Gan, and Y.-Q. Qi, 2004: Entropy budget of the ocean system. Geophys. Res. Lett., Vol. 31, L14311, doi:10.1029/2004GL019921.